■ KNEE: RESEARCH

Proximal tibial strain in medial unicompartmental knee replacements

A BIOMECHANICAL STUDY OF IMPLANT DESIGN

C. E. H. Scott,
M. J. Eaton,
R. W. Nutton,
F. A. Wade,
P. Pankaj,
S. L. Evans

From Cardiff University, Cardiff, and the Royal Infirmary of Edinburgh, Edinburgh, United Kingdom

■ C. E. H. Scott, BSc, MRCSEd, MSc, BASK Knee Research Fellow
■ R. W. Nutton, FRCS, MD, Consultant Orthopaedic Surgeon
■ F. A. Wade, FRCS, Consultant Orthopaedic Surgeon
Royal Infirmary of Edinburgh, 51 Little France Crescent, Old Dalkeith Road, Edinburgh EH16 4SA, UK.

■ M. J. Eaton, BEng, PhD, Research Associate
■ S. L. Evans, BEng, PhD, Professor
Cardiff University, Institute of Mechanical and Manufacturing Engineering, Cardiff School of Engineering, Queen's Buildings, The Parade, Cardiff CF24 3AA, UK.

■ P. Pankaj, PhD, Reader in Numerical Modelling
University of Edinburgh, School of Engineering, Alexander Graham Bell Building, Mayfield Road, Edinburgh EH9 3JL, UK.

Correspondence should be sent to Ms C. E. H. Scott; e-mail: chloe.scott@nhslothian.scot.nhs.uk

doi:10.1302/0301-620X.95B10.31644 $2.00

Bone Joint J 2013;95-B:1339–47.
Received 15 January 2013; Accepted after revision 4 June 2013

As many as 25% to 40% of unicompartmental knee replacement (UKR) revisions are performed for pain, a possible cause of which is proximal tibial strain. The aim of this study was to examine the effect of UKR implant design and material on cortical and cancellous proximal tibial strain in a synthetic bone model. Composite Sawbone tibiae were implanted with cemented UKR components of different designs, either all-polyethylene or metal-backed. The tibiae were subsequently loaded in 500 N increments to 2500 N, unloading between increments. Cortical surface strain was measured using a digital image correlation technique. Cancellous damage was measured using acoustic emission, an engineering technique that detects sonic waves ('hits') produced when damage occurs in material.

Anteromedial cortical surface strain showed significant differences between implants at 1500 N and 2500 N in the proximal 10 mm only ($p < 0.001$), with relative strain shielding in metal-backed implants. Acoustic emission showed significant differences in cancellous bone damage between implants at all loads ($p = 0.001$). All-polyethylene implants displayed 16.6 times the total number of cumulative acoustic emission hits as controls. All-polyethylene implants also displayed more hits than controls at all loads ($p < 0.001$), more than metal-backed implants at loads ≥ 1500 N ($p < 0.001$), and greater acoustic emission activity on unloading than controls ($p = 0.01$), reflecting a lack of implant stiffness. All-polyethylene implants were associated with a significant increase in damage at the microscopic level compared with metal-backed implants, even at low loads. All-polyethylene implants should be used with caution in patients who are likely to impose large loads across their knee joint.

Cite this article: *Bone Joint J* 2013;95-B:1339–47.

Unicondylar knee replacement (UKR) forms 8.7% of all primary knee arthroplasties recorded on the National Joint Registry (NJR) for England and Wales in the last ten years,[1] of which approximately 90% were for the medial compartment.[2] National joint registries have reported ten-year survival rates of UKR at around 90%[1,3-6] and case series have described ten-year survival rates between 80% and 96%, with considerable variation between implants and institutions.[2,7-11] Many registries have found unexplained pain to be a leading cause of UKR revision, [1,4,10,8] with a peak incidence at two years post-operatively.[3] Increased proximal tibial strain with structural damage and adaptive remodelling may contribute to this unexplained pain.[12] There is a paucity of biomechanical evidence to inform decisions between implants of different materials or geometries,[13] and the effect of implant design on proximal tibial strain remains poorly investigated.

Digital image correlation (DIC) is a non-destructive optical technique for the measurement of surface strain, involving applying a high-contrast speckle pattern to a sample and observing the pattern of deformation on loading using cameras. Rigid body movement is accounted for and excluded. DIC has been used to measure macroscopic and microscopic surface strain in both cadaver[14] and synthetic bone.[15]

Acoustic emission (AE) is a technique for measuring structural damage at the microscopic level. Damage in response to stress creates elastic sound waves that, after being conducted through material, can be detected at its surface by piezoelectric sensors, transforming the signal into a voltage and enabling real-time detection and quantification.[16,17] It has been used to investigate the properties of both cortical and cancellous bone,[18,19] including fracture healing and callus formation,[17] the location and propagation of cement fatigue cracks, the integrity of bone–cement interfaces[16] and loosening of hip prostheses.[20]

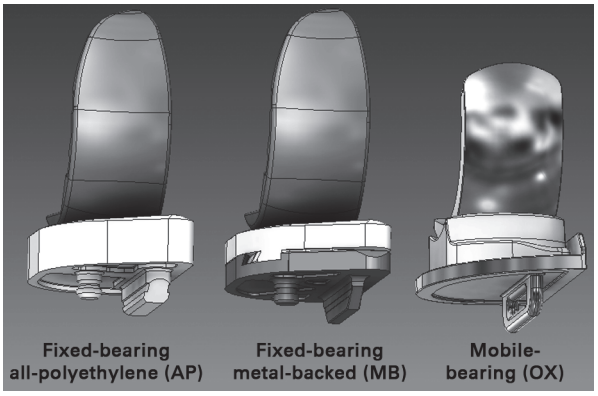

Fig. 1

Diagrams showing the geometry and under-surface projections of the all-polyethylene (AP) and metal-backed (MB) Sigma Partial fixed-bearing unicompartmental knee replacements (UKRs) and the Oxford (OX) mobile-bearing UKR. The fixed-bearing femur is polyradial and the mobile-bearing femur has a single radius common to two planes.

Both DIC and AE have been validated using micro-CT (μCT) *in vivo* and in synthetic bones.[14,16] AE is preferable to μCT for detecting peri-prosthetic structural damage, as some microscopically visible cracks close on unloading and may be missed on μCT in unloaded conditions.

The aims of this study were to determine the effect of medial UKR metal backing and the design of bearings on proximal tibial strain. DIC was used to measure cortical surface strain and AE was used to measure cancellous bone damage.

Materials and Methods

For this study we used 20 fourth-generation left-sided medium composite Sawbone tibiae (Pacific Research Laboratories, Vashon, Washington). These have < 10% interspecimen variability and material properties and mechanical behaviour similar to those of human cadaver bone.[21] Rigid polyurethane foam (Young's modulus E = 0.155 GPa) simulates cancellous bone and the short fibre-filled epoxy composite (E = 16.7 GPa) simulates cortical bone.

The Oxford Partial Knee (Biomet, Swindon, United Kingdom) is a mobile-bearing UKR and accounted for 68% of usage in 2011 in England and Wales,[22] Scandinavia[3,5] and Australasia.[4,6] The second most common UKR recorded by the NJR in 2011 was the Sigma Partial (DePuy, Johnson & Johnson Professional Inc., Raynham, Massachusetts), constituting 13% of usage.[22] This is a fixed-bearing non-conforming implant with both all-polyethylene (AP) and metal-backed (MB) tibial options. Both AP and MB tibial components have a keel and a peg, the only geometric differences being a wider keel in the AP implant (AP 5 mm, MB 2.55 mm) and greater under-surface offset in the AP (AP 1 mm, MB 0.5 mm) (Fig. 1). Both designs are manufactured in cobalt–chromium alloy (E = 210 GPa). A single size-3 Sigma Partial femur, five size 3 MB tibiae with an 8-mm matched tibial insert, and five size-3 8-mm AP tibiae were tested, as well as a single medium Oxford femoral component (OX) with five size-C tibiae and a 4 mm polyethylene bearing were used. Five tibiae were allocated to each of the three implant groups and five were used as controls (TIB).

In order to ensure uniformity of specimens, horizontal and vertical proximal tibial cuts were measured using anatomical axes and landmarks and cut without using implant-specific instrumentation. In the sawbones the medial proximal tibial angle (MPTA) and the posterior tibial slope (PTS) was 87° and 7°, respectively. Both implants define an optimal frontal plane alignment as an MPTA of 90° and sagittal alignment reproducing native PTS (here 7°). Tibial coronal and sagittal plane anatomical axes were defined according to Paley,[23] and were drawn onto the tibiae proximally. All cuts were referenced from these axes, and 6 mm of tibia were resected to restore the joint line with MPTA 90° and PTS 7°. The depth of the resected tibia, the MPTA and PTS were measured to monitor specimen uniformity. Cut tibiae were randomly assigned to each study group. Implant-specific instrumentation was used for subsequent preparation, and implants were cemented using Smart-Set High Viscosity polymethylmethacrylate bone cement (DePuy, Warsaw, Indiana) with a cement mantle of 1 mm to 1.5 mm. Mantle thickness was measured at three locations in each specimen using a digital calliper: the anterior corner of the implant, the posterior corner and the medial line present on all tibiae from manufacturing.

Femoral components were cemented onto custom-designed blocks made of hard wood and steel to facilitate loading directly over the point of contact in 30° of flexion. For the control tibiae, the distal 30 mm of a Sawbone composite femur was cut to represent a 30° articulation. In order to simulate intervening articular cartilage and meniscus in controls, a 6 mm thick piece of Sorbothane 75 durometer polyurethane (Sorbothane Inc., Kent, Ohio) was interposed between the femoral and tibial surfaces prior to loading. Sorbothane is a viscoelastic polymeric solid with a Young's modulus from 0.83 MPa to 2.07 MPa (cartilage: E = 0.31 to 1.13 MPa[24]). The line of loading was drawn on the femoral component assemblies and aligned with the midpoint of the tibial component in the sagittal plane to reproduce 30° of flexion.[25] In the mobile-bearing implant the bearing was aligned with the centre of the tibial base plate.

Distally, coronal and sagittal mechanical axes were drawn onto the tibiae to aid alignment of the experimental set-up. A steel coupling cylinder was inserted vertically into the tibial plafond and the tibia was mounted on a ball bearing as a simply supported construct (Fig. 2). Anterolateral constraints were applied at the mid-tibia to prevent displacement of the tibia on loading. Medial plateau loading was achieved via a 5 kN servohydraulic loading machine (Losenhausen Maschinenbau, Dusseldorf, Germany). A pre-load of 100 N was applied to check the set-up. Loading was then undertaken in 500 N increments to a maximum of 2500 N, unloading between increments to 100 N. The loading rate was 5 mm/min, and load data were recorded every 0.1 s.

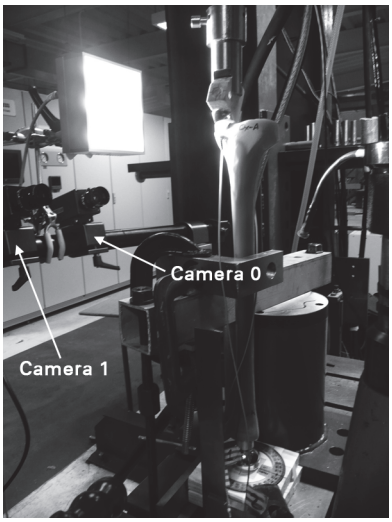

Fig. 2

Photograph showing the experimental set-up with camera positions.

Cortical bone strain – digital image correlation. The proximal tibia was coated with matt white paint and a black speckle pattern was applied (Fig. 3). Paint was removed at two locations on the anterior and posterior surfaces and two AE sensors were attachment with cyanoacrylate adhesive. Two charge-coupled DIC cameras (Limess, Messtechnik und Software GmbH, Krefeld, Germany) were positioned to view the anteromedial tibia (Fig. 2). A red light source was used to maximise speckle contrast. The displacement of pixel regions relative to surrounding regions is analysed using computer software to represent the magnitude, gradient and distribution of strain across a surface. Cameras were calibrated and images taken at zero load, 100 N pre-load and at each 500 N load and after loading, giving a total of 12 images for each specimen loaded up to 2500 N.

Analysis was performed using Istra 4D 3.1 software (Dantec Dynamics, Skovlunde, Denmark). A contour statistical error radius map of the pre-load image was used to apply a mask over the area where resolution was < 0.001 mm. This mask determined the area over which surface strain was examined in all images in the specimen series (Fig. 3). Strain was visualised as vertical strain in the *y*-direction from –5000 to +5000 με (microstrain). For quantitative analysis, a line was drawn from the cut surface of the tibia (or the equivalent depth in controls) down the anteromedial cortex 5 mm anterior to the standard hole present in each tibia using the camera. This was divided into 5 mm depth zones to a maximum of 30 mm. This 30 mm length contained strain data at ≥ 80 consecutive points, with each 5 mm increment containing approximately 12 consecutive data points. Data were exported to Excel 2010 (Microsoft, Redmond, Washington) for onward analysis.

Cancellous damage – acoustic emission. Two piezoelectric Pancom Pico-z AE sensors (125 to 750 kHz; Pancom, Huntingdon, United Kingdom)[26] were affixed in equivalent positions on each tibia using cyanoacrylate adhesive (Fig. 3). Sensors were connected to IL40S pre-amplifiers (Physical Acoustics Corporation, Princeton, New Jersey) with 40 dB gain and 20 to 1200 kHz bandwidth. For computer analysis a Physical Acoustics Corporation processor was used with AEWin 3.5 software (Physical Acoustics Corporation). Sensor coupling was assessed using a Hsu-Nielson (H-N) source,[27] and the response of all sensors was seen to be > 97 dB. The data were recorded continuously throughout the loading cycle. The AE data were marked at the start of each loading phase, at load hold, and at the start of each unload. For each acoustic hit > 45 dB the following parameters were recorded: peak amplitude, duration, rise time, ring-down counts (number of threshold crossings) and absolute energy (atto-Joules (aJ)). Data so obtained were exported to Excel 2010 for onward analysis.

Statistical analysis. Analysis was performed using IBM-SPSS v19.0 (SPSS Inc., Chicago, Illinois). Continuous parametric data (quantitative DIC data) were analysed using one-way analysis of variance (ANOVA) to compare implant types, and a two-tailed independent Student's *t*-test to compare implants and controls. Non-parametric data (AE data) were analysed using the Kruskal–Wallis test to compare means between implants, and Mann–Whitney U tests to compare implants and controls. A p-value < 0.05 was deemed significant.

Results

The implantation method produced standardised tibial resections, prosthesis alignment and cement mantles (Table I). The mean contact area of the fixed-bearing implants was 116 mm^2 (SD 20.0; 68 to 144). There was no significant difference in mean contact area between AP and MB implants (114.4 mm^2 (SD 28.9) *vs* 117.6 mm^2 (SD 7.8); p = 0.752, Mann–Whitney). The contact area of the fully conforming mobile-bearing implant was approximately 665 mm^2.

Digital image correlation. By eye, there was little difference in vertical surface strain between implants and controls; an example of the image is seen in Figure 3. In a quantitative analysis of strain at 1500 N and 2500 N (Table II, Fig. 4), no implant reproduced the tensile vertical strain of the proximal control tibiae. At 1500 N, one-way ANOVA showed significant differences in surface strain between the implant groups at depths of 0 to 5 mm (p < 0.001), 5 to 10 mm (p < 0.001) and 25 to 30 mm (p = 0.037). At 2500 N, one-way ANOVA showed significant differences between implant groups at depths of 0 to 5 mm (p < 0.001), 5 to 10 mm (p < 0.001), 10 to 15 mm (p = 0.041), 20 to 25 mm (p = 0.026) and 25 to 30 mm (p = 0.011). Significant differences existed between all implants and controls at loads of 1500 N and 2500 N for the proximal 5 mm only (Table II). Significant differences in compressive strain exist between MB implants and controls at 25 to 30 mm only where the

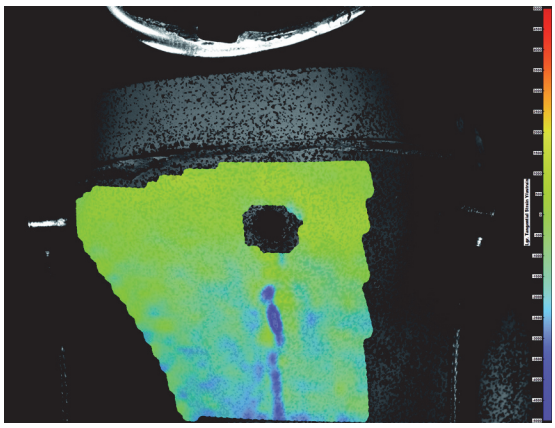

Fig. 3a

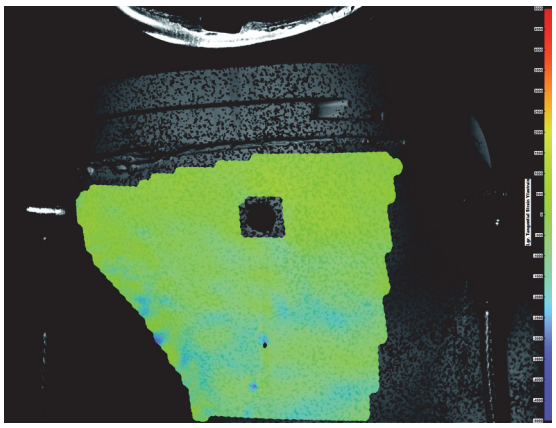

Fig. 3b

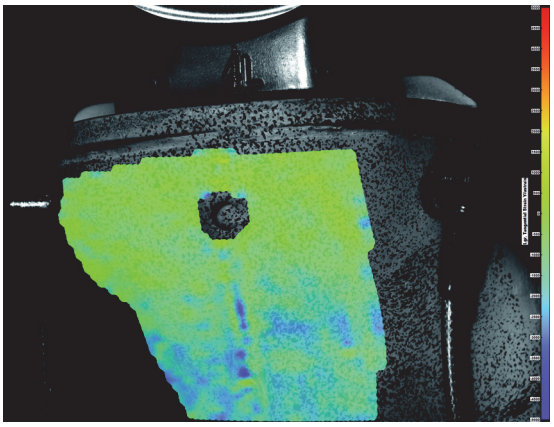

Fig. 3c

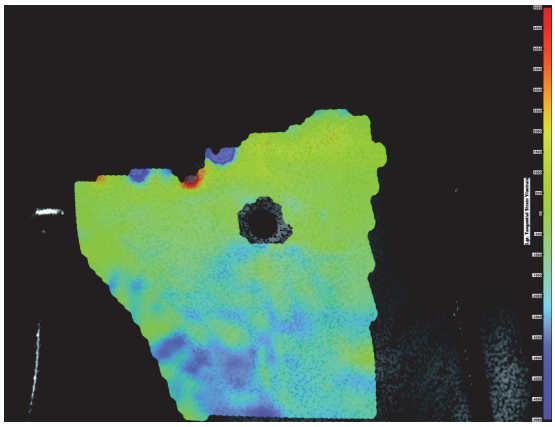

Fig. 3d

Digital image correlation (DIC) figures from camera 1 displaying vertical strain in the*y*-direction (–5000 to +5000 με window) at a 2500 N load in a) an all-polyethylene (AP) implant, b) a metal-backed implant, c) the Oxford mobile-bearing implant, and d) the control tibia. The area is defined by a specimen-specific mask to maximise accuracy. The acoustic emission (AE) sensors are affixed to anterior and posterior cortices. Compressive strain appears blue and tensile strain red.

Table I. Tibial component alignment, resection and cement mantles in all specimens

	Specimen†			
Mean (SD) parameter*	**AP**	**MB**	**OX**	**p-value**
MPTA (°)	89.8 (0.45)	90 (0)	89.6 (0.89)	0.581‡
PTS (°)	6.4 (0.89)	6.6 (0.55)	6.6 (0.89)	0.857‡
Resection (mm)				
Medial	6.23 (0.44)	6.10 (0.19)	6.48 (0.18)	0.125‡
Minimum	6.01 (0.55)	6.02 (0.20)	6.03 (0.54)	0.961‡
Cement mantle (mm)				
Anterior	1.35 (0.18)	1.35 (0.27)	1.37 (0.12)	0.988§
Medial	0.94 (0.24)	1.14 (0.07)	1.18 (0.23)	0.154§
Posterior	1.64 (0.10)	1.50 (0.45)	1.70 (0.26)	0.570§

* MPTA, medial proximal tibial angle; PTS, posterior tibial slope
† AP, all-polyethylene; MB, metal-backed; OX, Oxford mobile-bearing component
‡ Kruskal–Wallis test
§ one-way analysis of variance

metal backing produced relative shielding. Only the fixed-bearing MB implant does not breach the physiological strain limits of -1500 to +1500 με at loads of 2500 N.

Acoustic emission. Of the AE activity, 60% to 70% was detected at the posterior sensor in all groups. The hit amplitude and number for each implant type throughout the loading cycle are shown in Figure 5. The cumulative number of AE hits up to a 2500 N load differed significantly between implants (p = 0.001 Kruskal–Wallis). AP implants displayed 352 mean cumulative hits (SD 74.3), MB 140 (SD 19.9), OX 63 (SD 29.4) and controls 23 (SD 11.6). High hit rates were associated with high absolute energies.

Table II. The mean vertical strain for each implant at each depth zone compared with that of the intact tibia controls at 1500 N and 2500 N loads. Positive strain values represent tensile strain, and negative values compressive strain (CI, confidence interval)

Implant/Zone (mm)*	Mean (SD) strain (με)	% of control strain	p-value (*vs* control)†	95% CI of vertical microstrain
1500 N LOAD				
AP				
0 to 5	145 (142)	25.4	0.002	-640 to -208
5 to 10	324 (173)	-531.1	0.003	169 to 601
10 to 15	-546 (139)	200.0	0.015	-476 to 69
15 to 20	-937 (142)	119.7	0.106	-348 to 40
20 to 25	-1066 (55)	102.0	0.807	-222 to 178
25 to 30	-1130 (55)	93.7	0.344	-98 to 252
MB				
0 to 5	154 (142)	27.1	0.002	-631 to -199
5 to 10	357 (84)	-585	< 0.001	269 to 568
10 to 15	-311 (161)	113.9	0.710	-256 to 183
15 to 20	-742 (288)	94.8	0.773	-281 to 365
20 to 25	-850 (320)	81.4	0.262	-196 to 586
25 to 30	-872 (336)	72.3	0.087	-63 to 732
OX				
0 to 5	-168 (61)	-29.0	< 0.001	-932 to -542
5 to 10	-280 (208)	459	0.086	-477 to 41
10 to 15	-450 (188)	165	0.148	-433 to 80
15 to 20	-640 (149)	81.7	0.158	-71 to 358
20 to 25	-974 (59)	93.3	0.344	-98 to 239
25 to 30	-908 (7)	75.3	0.014	99 to 498
2500 N LOAD				
AP				
0 to 5	550 (280)	58.6	0.037	-746 to -30
5 to 10	632 (324)	-482.4	0.004	366 to 1158
10 to 15	-813 (194)	172.2	0.010	-574 to -106
15 to 20	-1503 (256)	123.4	0.104	-645 to 73
20 to 25	-1827 (207)	108.0	0.397	-486 to 214
25 to 30	-1745 (133)	91.0	0.230	-132 to 476
MB				
0 to 5	255 (199)	27.2	0.001	-978 to -389
5 to 10	513 (123)	-391	< 0.001	457 to 831
10 to 15	-412 (285)	87.3	0.673	-257 to 378
15 to 20	-1145 (357)	94.0	0.714	-369 to 514
20 to 25	-1289 (289)	76.2	0.052	-4 to 809
25 to 30	-1301 (328)	67.8	0.017	150 to 1081
OX				
0 to 5	-182 (40)	-19.4	< 0.001	-1422 to -819
5 to 10	-345 (123)	264	0.063	-494 to 16
10 to 15	-683 (247)	144.7	0.145	-518 to 97
15 to 20	-1200 (301)	98.5	0.932	-446 to 480
20 to 25	-1676 (99)	99.0	0.926	-389 to 420
25 to 30	-1662 (32)	86.7	0.157	-131 to 642

* AP, all-polyethylene; MB, metal-backed; OX, Oxford mobile-bearing component
† paired *t*-test

On loading, there were significant differences in the number of AE hits between implants at every load (500 N to 2500 N) (Table III) (Fig. 6). Compared with controls (TIB), AP implants had significantly more hits at all loads, the MB implants at loads ≥ 1500 N, and the OX at 1500 N and 2000 N loads only ($p < 0.001$, Mann–Whitney). Compared with OX, AP implants had significantly more hits at loads ≥ 1500 N ($p < 0.001$, Mann–Whitney). There were no significant differences in AE hits number between MB and OX implants at any load. The absolute energy associated with AE hits differed significantly between implants at loads of 1500 N and 2000 N (Table III). Compared with controls, AP implants had significant differences in absolute energy emissions at 2000 N ($p < 0.001$ Mann–Whitney).

Significant differences in AE activity were also found on unloading from 2000 N ($p = 0.010$) and 2500 N ($p = 0.011$, Kruskal–Wallis) (Table IV, Fig. 6b). No significant differences existed in unloading from lower loads (500 N, $p = 0.392$; 1000 N, $p = 0.071$; 1500 N, $p = 0.063$). AP implants displayed significantly more AE hits than

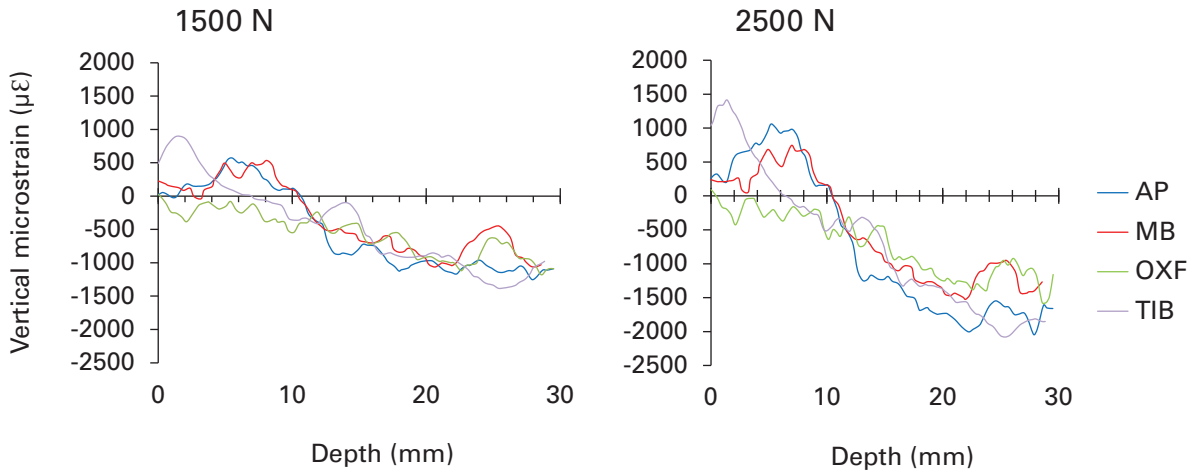

Fig. 4

Graphs showing the mean vertical surface microstrain for all specimens of each implant type on digital image correlation at loads of 1500 N (left) and 2500 N (right) (AP, all-polyethylene; MB, metal-backed; OXF, Oxford mobile-bearing; TIB, control tibia).

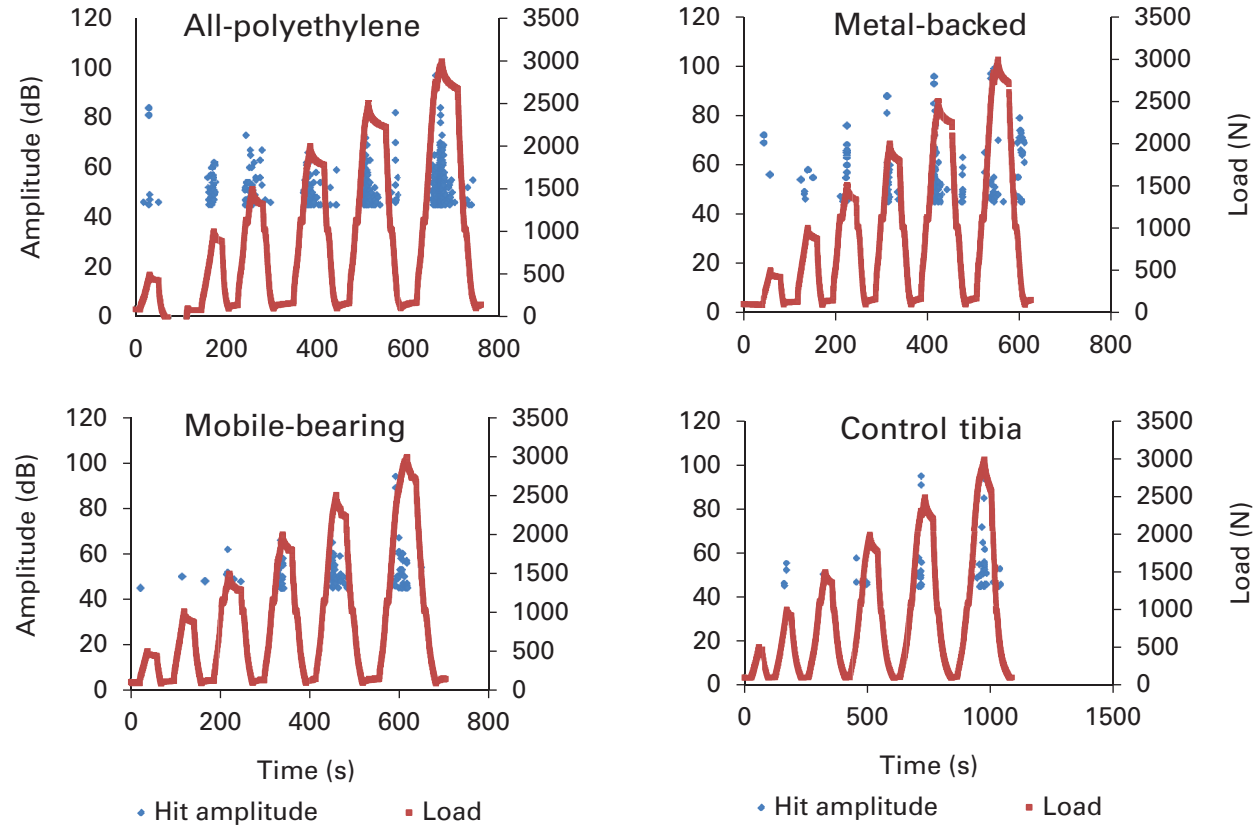

Fig. 5

Sample graphs of the continuous acoustic emission (AE) output graphs showing hit amplitude and load for a specimen of each implant type. Each AE hit is represented by a single blue point and load every 0.1 second by a single red point. A graph for each implant type is shown.

controls on unloading from 2000 N ($p < 0.001$, Mann–Whitney) and more than the mobile-bearing OX on unloading from 2500 N ($p < 0.001$, Mann–Whitney). AE hits on unloading the MB implant from 2500 N were significantly greater than in OX implants ($p < 0.001$, Mann–Whitney), but not greater than in controls ($p = 0.055$).

Discussion

Our findings show significant differences in proximal tibial strain and damage in synthetic composite bone models between metal-backed and all-polyethylene tibial components in medial UKRs. Metal-backed implants are associated with a significant strain shielding effect at a depth of

Table III. Number of acoustic emission (AE) hits and associated absolute energy on loading by implant

	Implant*				
	AP	**MB**	**OX**	**Control tibiae**	**p-value†**
Mean (SD) AE hits (n)					
500 N load	9.40 (4.77)	2.80 (2.59)	1.60 (2.07)	0.60 (0.89)	0.010
1000 N load	24.40 (8.38)	11.80 (16.53)	4.80 (6.94)	1.60 (1.82)	0.012
1500 N load	96.00 (61.08)	15.00 (5.52)	9.60 (8.17)	1.00 (1.00)	0.001
2000 N load	70.80 (14.10)	39.00 (18.88)	19.40 (9.61)	2.40 (2.51)	0.001
2500 N load	104.80 (36.90)	53.60 (14.26)	23.20 (8.70)	12.60 (10.31)	0.001
Mean (SD) absolute energy (aJ)					
500 N load	1.92E+05 (2.60E+05)	8.59E+04 (1.14E+05)	1.03E+06 (2.18E+06)	2.31E+03 (5.12E+03)	0.182
1000 N load	2.83E+05 (5.87E+05)	4.51E+05 (1.00E+06)	7.49E+04 (1.12E+05)	6.08E+04 (1.36E+05)	0.213
1500 N load	3.26E+06 (5.27E+06)	2.26E+05 (2.49E+05)	6.45E+05 (1.44E+06)	9.85E+03 (2.19E+04)	0.013
2000 N load	1.55E+07 (3.46E+07)	5.03E+05 (5.10E+05)	5.12E+03 (5.27E+03)	1.59E+02 (2.00E+02)	0.002
2500 N load	7.71E+06 (1.72E+07)	1.71E+06 (1.90E+06)	8.75E+06 (1.96E+07)	2.14E+07 (3.07E+07)	0.548

* AP, all-polyethylene; MB, metal-backed; OX, Oxford mobile-bearing component
† Kruskal–Wallis test

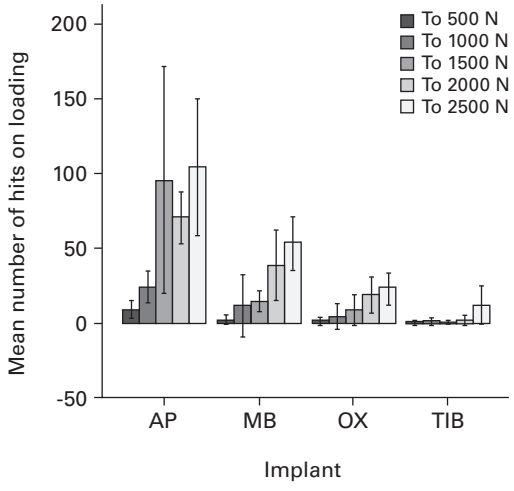

Fig. 6a

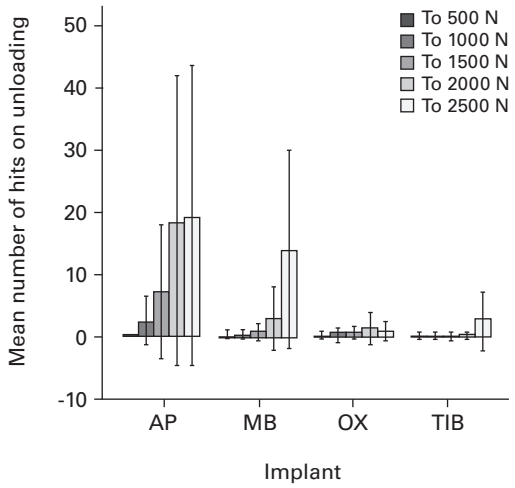

Fig. 6b

Graphs showing the mean number of hits (as measured on acoustic emission) by implant type and load on a) loading and b) unloading. The error bars denote the 95% confidence intervals (AP, all-polyethylene; MB, metal-backed; OX, Oxford mobile-bearing; TIB, control tibia).

5 mm to 10 mm below the implant. The most striking differences between implants, however, occurred when measuring cancellous damage using AE.

Composite Sawbone models have been validated as being representative of cadaver bone on biomechanical testing.[21,28] Unlike cadaver specimens they display little interspecimen variability, and can therefore provide reproducible results.[21] These models are widely used in the biomechanical literature to test implant and construct viability and to validate finite element models, facilitating additional study.[29,30] In synthetic bone, micro-CT has validated AE activity with actual damage, with high-amplitude hits signifying greater damage.[16] Leung et al[16] found that AE detected and located early failure in synthetic bone, where hits of > 70 dB amplitude were associated with cracks of > 50 μm, and hits of > 90 dB caused critical damage of crack length 1 mm to 5 mm. AE activity in cadaver bone has also been validated with micro-CT as being representative of actual cancellous microfracture,[31] with high-amplitude emissions indicating fracture.[32] Although cracks may not propagate identically through cadaver and synthetic bone owing to the trabecular microstructure of cadaver bone, these studies have shown that high amplitudes and high energies reflect significant damage in both.[31-33] Although there appear to have been no direct comparisons of AE activity between cadaver bone and synthetic bone in the literature, some of their failure characteristics have been shown to be similar.[34]

Only the Oxford UKR has been reported in finite element analyses (FEAs), where a 40% increase in proximal tibial bone strain is reported.[12] One mechanical testing study has been reported[13] using DIC with photoelastic

Table IV. Number of acoustic emission (AE) hits and associated absolute energy on unloading by implant

	Implant*				
	AP	**MB**	**OX**	**Control tibiae**	**p-value†**
Mean (SD) AE hits (n)					
500 N (unloading)	0	0	0	0.20 (0.45)	0.392
1000 N (unloading)	2.60 (3.13)	0.40 (0.55)	0.80 (0.45)	0.20 (0.45)	0.071
1500 N (unloading)	7.20 (8.64)	0.80 (1.10)	0.80 (0.84)	0.20 (0.45)	0.063
2000 N (unloading)	18.20 (18.36)	3.00 (4.06)	1.40 (2.07)	0.20 (0.45)	0.010
2500 N (unloading)	19.00 (18.99)	13.80 (12.72)	1.00 (1.22)	2.80 (3.90)	0.011
Mean (SD) absolute energy (aJ)					
500 N (unloading)	0	0	0	3.53E+01 (7.88E+01)	0.392
1000 N (unloading)	1.12E+02 (1.59E+02)	2.01E+01 (4.02E+01)	9.27E+01 (1.13E+02)	1.19E+01 (2.67E+01)	0.164
1500 N (unloading)	1.07E+03 (1.21E+03)	3.77E+01 (5.95E+01)	1.82E+03 (4.04E+03)	2.21E+00 (4.94E+00)	0.114
2000 N (unloading)	5.18E+03 (5.54E+03)	4.14E+03 (9.03E+03)	3.11E+01 (4.89E+01)	2.34E+01 (5.24E+01)	0.029
2500 N (unloading)	3.44E+04 (5.43E+04)	4.19E+04 (4.55E+05)	3.48E+01 (4.44E+01)	1.80E+04 (3.88E+04)	0.017

* AP, all-polyethylene; MB, metal-backed; OX, Oxford mobile-bearing component
† Kruskal–Wallis test

Table V. Loads applied with corresponding body weight (BW) values for an 80 kg person (the mean weight of patients undergoing unicompartmental knee replacement at our institution), including medial compartment correction for 57%, and the corresponding physical activity from the literature.[36-38] Gravity constant = 9.8065 m/s^2, 1BW = 785 N

Load (N)	%BW (absolute)	%BW (corrected)	Activity
500	60	110	Cycling
1000	130	220	
1500	190	330	Level walking, chair rising
2000	260	440	Uphill walking
2500	325	550	Stair descent
3000	390	660	Downhill walking

paint to compare the Oxford implant with a fixed-bearing AP implant at loads of 1500 N. Surface shear strain appeared to be significantly greater in the AP implant.

High-amplitude hits occurred with greater frequency, and at lower loads, in the AP implants than in both metal-backed implants and controls, and hits were of high absolute energies even at low loads. Metal-backed implants produced high energies at high loads only. AP implants also produced significant amounts of AE activity on unloading. This probably reflects bending of the polyethylene on loading,[35] with elastic recoil on unloading causing further damage.

Stiffer implants subside without bending. Stiffness is a function of both material properties and geometry, and the MB implant with 1.54 mm of metal backing is less stiff, allowing more bending and creating more damage, than the OX implant with 2.5 mm thick metal backing, and this is reflected in their AE differences on unloading. The thinner, less stiff fixed-bearing metal base plate is associated with more cumulative hits on loading and unloading, more energy, and more hits of greater amplitude than the stiffer Oxford implant with thicker metal backing.

In vivo measurements of load in TKR show 290% to 345% body weight (BW) (mean 316%) passes across the knee in 35° of flexion during stair climbing[36]; 57% of this total load passes through the medial compartment, and load is maximal at 35°.[37] Table V shows that the tibiofemoral loads applied in this study were compatible with equivalent activities.[36-38] Loading up to 2500 N was representative of physiological conditions. Load was applied to the medial compartment, similar to the study by Small et al.[13] This was thought to be representative of a worst-case scenario and prevented lateral artefact from influencing AE readings. Loads were applied at 5 mm/min, a strain rate associated with favourable bone properties.[19] Implants were loaded centrally, the point of contact identified as appropriate by the available kinematic data.[25]

Limitations of this study include the use of synthetic, rather than cadaveric bone. This was necessary to standardise conditions and evaluate the effect of the implant alone. The control tibiae were loaded with interposing simulated soft tissue, which may have had an excessive cushioning effect. The necessary mid-tibial constraint may have introduced bending moments. The region imaged with DIC excluded anterior and posterior regions where strain may be concentrated.

In conclusion proximal strain shielding occurs in metal-backed implants and the thickness of the metal backing affects cancellous bone damage at the microscopic level. All-polyethylene medial UKR implants are associated with significantly more cancellous damage than metal-backed

implants, even at low loads in our experimental system. Implant stiffness is affected by both material properties and geometry, and this should be considered in implant selection. The clinical importance of elevated tibial strain and contribution to pain requires further investigation.

This research was supported by grants from the British Association for Surgery of the Knee and Joint Action. Implants were provided by Biomet UK and DePuy Synthes who had no other involvement with the study.

The authors would like to thank Professor H. Simpson and Mr C. Howie for the use of the Edinburgh Orthopaedic Engineering Centre to implant all of the tibiae; Mr M. Moran and Mr G. Dall for the cement; and Dr R. Wallace, A. MacLeod and N. Conlisk for Orthopaedic Engineering support in Edinburgh.

No benefits in any form have been received or will be received from a commercial party related directly or indirectly to the subject of this article.

This article was primary edited by D. Rowley and first-proof edited by G. Scott.

References

1. **No authors listed.** National Joint Registry for England and Wales. Ninth Annual Report, 2012. http://www.njrcentre.org.uk (date last accessed 5 June 2013).
2. **Lewold S, Robertsson O, Knutson K, Lidgren L.** Revision of unicompartmental knee replacement: outcome in 1,135 cases from the Swedish Knee Arthroplasty study. *Acta Orthop Scand* 1998;69:469–474.
3. **No authors listed.** Annual Report of the Norwegian Arthroplasty Register, 2010. http://nrlweb.ihelse.net/eng/Report_2010.pdf (date last accessed 5 June 2013).
4. **Rothwell A, Taylor J, Wright M, et al.** New Zealand Orthopaedic Association: The New Zealand Joint Registry twelve year report, 2011. http://nzoa.org.nz/system/files/NJR%2012%20Year%20Report%20Jan%2099%20-%20Dec%202010.pdf (date last accessed 5 June 2013).
5. **No authors listed.** The Swedish Knee Arthroplasty Register Annual Report, 2011. http://www.knee.nko.se/english/online/uploadedFiles/115_SKAR2011_Eng1.0.pdf (date last accessed 5 June 2013).
6. **No authors listed.** Australian Orthopaedic Association: National Joint Replacement Registry: Annual Report 2012. https://aoanjrr.dmac.adelaide.edu.au/annual-reports-2012 (date last accessed 5 June 2013).
7. **Svärd UC, Price AJ.** Oxford medial unicompartmental knee arthroplasty: a survival analysis of an independent series. *J Bone Joint Surg [Br]* 2001;83-B:191–194.
8. **Furnes O, Espehaug B, Lie SA, et al.** Failure mechanisms after unicompartmental and tricompartmental primary knee replacement with cement. *J Bone Joint Surg [Am]* 2007;89-A:519–525.
9. **Newman J, Pydisetty RV, Ackroyd C.** Unicompartmental or total knee replacement: the 15-year results of a prospective randomised controlled trial. *J Bone Joint Surg [Br]* 2009;91-B:52–57.
10. **Pandit H, Jenkins C, Gill HS, et al.** Minimally invasive Oxford phase 3 unicompartmental knee replacement: results of 1000 cases. *J Bone Joint Surg [Br]* 2010;93-B:198–204.
11. **Bhattacharya R, Scott CE, Morris HE, Wade F, Nutton RW.** Survivorship and patient satisfaction of a fixed bearing unicompartmental knee arthroplasty incorporating an all-polyethylene tibial component. *Knee* 2012;19:348–351.
12. **Simpson DJ, Price AJ, Gulati A, Murray DW, Gill HS.** Elevated proximal tibial strains following unicompartmental knee replacement: a possible cause of pain. *Med Eng Phys* 2009;31:752–757.
13. **Small SR, Berend ME, Ritter MA, Buckley CA, Rogge RD.** Metal backing significantly decreases tibial strains in a medial unicompartmental knee arthroplasty model. *J Arthroplasty* 2011;26:777–782.
14. **Christen D, Levchuk A, Schori S, et al.** Deformable image registration and 3D strain mapping for the quantitative assessment of cortical bone microdamage. *J Mech Behav Biomed Mater* 2012;8:184–193.
15. **Tayton E, Evans S, O'Doherty D.** Mapping the strain distribution on the proximal femur with titanium and flexiable-stemmed implants using digital image correlation. *J Bone Joint Surg [Br]* 2010;92-B:1176–1181.
16. **Leung SY, New AM, Browne M.** The use of complementary non-destructive evaluation methods to evaluate the integrity of the cement-bone interface. *Proc Inst Mech Eng H* 2009;223:75–86.
17. **Hirasawa Y, Takai S, Kim WC, et al.** Biomechanical monitoring of healing bone based on acoustic emission technology. *Clin Orthop Relat Res* 2002;402:236–244.
18. **Nicholls PJ, Berg E.** Acoustic emission properties of callus. *Med Biol Eng Comput* 1981;19:416–418.
19. **Wells JG, Rawlings RD.** Acoustic emission and mechanical properties of trabecular bone. *Biomaterials* 1985;6:218–224.
20. **Mavrogordato M, Taylor M, Taylor A, Browne M.** Real time monitoring of progressive damage during loading of a simplified total hip stem construct using embedded acoustic emission sensors. *Med Eng Phys* 2011;33:395–406.
21. **Cristofolini L, Viceconti M.** Mechanical validation of whole bone composite tibia models. *J Biomech* 2000;33:279–288.
22. **No authors listed.** National Joint Registry. Prostheses used in hip, knee and ankle replacements 2011, 2012. http://www.njrcentre.org.uk/njrcentre/Portals/0/Documents/England/Reports/9th_annual_report/Prostheses%20used%20in%20hip%20knee%20and%20ankle%20replacements%202011.pdf (date last accessed 5 June 2013).
23. **Paley D.** Normal limb alignment and joint orientation. In: Herzenberg JE, Paley D, ed. *Principles of deformity correction.* Springer: Berlin, 2002:1–17.
24. **Korhonen RK, Laasanen MS, Töyräs J, et al.** Comparison of the equilibrium response of articular cartilage in unconfined compression, confined compression and indentation. *J Biomech* 2002;35:903–909.
25. **Li MG, Yao F, Joss B, et al.** Mobile vs. fixed bearing unicondylar knee arthroplasty: a randomized study on short term clinical outcomes and knee kinematics. *Knee* 2006;13:365–370.
26. **Eaton MJ, Pullin R, Holford KM.** Acoustic emission source location in composite materials using Delta T Mapping. *Composites Part A: Applied Science and Manufacturing* 2012;43:856–863.
27. **Hsu NN, Breckenridge FR.** Characterization and calibration of acoustic emission sensors. *Mater Eval* 1981;39:60–68.
28. **Bolder SB, Schreurs BW, Verdonschot N, et al.** Particle size of bone graft and method of impaction affect initial stability of cemented cups: human cadaveric and synthetic pelvic specimen studies. *Acta Orthop Scand* 2003;74:652–657.
29. **Completo A, Fonseca F, Simões JA.** Finite element and experimental cortex strains of the intact and implanted tibia. *J Biomech Eng* 2007;129:791–797.
30. **Gray HA, Zavatsky AB, Taddei F, Cristofolini L, Gill HS.** Experimental validation of a finite element model of a composite tibia. *Proc Inst Mech Eng H* 2007;221:315–324.
31. **Hasegawa K, Takahashi HE, Koga Y, et al.** Mechanical properties of osteopenic vertebral bodies monitored by acoustic emission. *Bone* 1993;14:737–743.
32. **Van Toen C, Street J, Oxland TR, Cripton PA.** Acoustic emission signals can discriminate between compressive bone fractures and tensile ligament injuries in the spine during dynamic loading. *J Biomech* 2012;45:1643–1649.
33. **Hymes RA, Levine M, Schulman JE, Westbrook R, Li J.** Mechanisms of failure of locked plate fixation of the proximal humerus: acoustic emissions as a novel assessment modality. *J Orthop Trauma* 2012:Epub.
34. **Zdero R, Olsen M, Bougherara H, Schemitsch EH.** Cancellous bone screw purchase: a comparison of synthetic femurs, human femurs, and finite element analysis. *Proc Inst Mech Eng H* 2008;222:1175–1183.
35. **Reilly D, Walker PS, Ben-Dov M, Ewald FC.** Effects of tibial components on load transfer in the upper tibia. *Clin Orthop Relat Res* 1982;165:273–282.
36. **Kutzner I, Heinlein B, Graichen F, et al.** Loading of the knee joint during activities of daily living measured in vivo in five subjects. *J Biomech* 2010;43:2164–2173.
37. **Zhao D, Banks SA, D'Lima DD, Colwell CW Jr, Fregly BJ.** In vivo medial and lateral tibial loads during dynamic and high flexion activities. *J Orthop Res* 2007;25:593–602.
38. **Kuster MS, Wood GA, Stachowiak GW, Gächter A.** Joint load considerations in total knee replacement. *J Bone Joint Surg [Br]* 1997;79-B:109–113.